SAND2016-10824C

Substructuring of Viscoelastic Subcomponents with Interface Reduction

Robert J. Kuether

Senior Member of Technical Staff, Sandia National Laboratories[1], P.O. Box 5800 MS 0346, Albuquerque, NM, USA 87185

Kevin L. Troyer

Senior Member of Technical Staff, Sandia National Laboratories[1], P.O. Box 5800 MS 0346, Albuquerque, NM, USA 87185

ABSTRACT

The Craig-Bampton approach for component mode synthesis in structural dynamics has been widely used to reduce the order of large, detailed finite element models made from linear elastic materials. This methodology separates the full order model into smaller subcomponents and reduces the equations of motion with a truncated set of fixed-interface modes and static constraint modes. A drawback of this approach is that the model has one constraint mode for every interface degree-of-freedom, which may result in a large and prohibitively costly superelement. Previous work has addressed this issue via characteristic constraint modes, which reduces the number of interface degrees-of-freedom by performing a secondary modal analysis on the interface partition. The current work extends the Craig-Bampton approach with interface reduction to include subcomponents with linear viscoelastic materials modeled using a Prony series. For substructures containing materials such as foams or polymers, the viscoelastic constitutive law more accurately represents the material energy dissipation compared to traditional viscous or modal damping. The new approach will be demonstrated on the assembly of two composite plates with fixed boundary conditions along one edge.

Keywords: *viscoelasticity, model reduction, substructuring, Prony series, structural dynamics*

1. Introduction

Component mode synthesis (CMS), or dynamic substructuring, has long been used as a model reduction technique in structural dynamics. The idea is to separate a large scale finite element model into smaller, more computationally manageable subcomponents and reduce them with a set of component mode shapes. These lower order subcomponent models are then coupled to provide an efficient and accurate reduced order model of the original structure. Many techniques have been developed over the past 60 or so years and the interested reader is directed to the review papers in [1, 2]. Some variations of the substructuring approaches include the use of free- or fixed- interface modes (or other hybrid methods), dual or primal assembly, and frequency or physical domain coupling. Many of the common CMS strategies are for linear, undamped structures with linear elastic constitutive laws, but fewer works have been developed for models incorporating nonlinear or time-dependent materials.

The focus of this research is to develop a fixed-interface substructuring approach using primal assembly in the physical domain for finite element models with linear viscoelastic constitutive laws modeled as Prony series. The work by Qian et al. [3] presented a substructure synthesis method for the second-order form of finite element

[1] Sandia National Laboratories is a multi-mission laboratory managed and operated by Sandia Corporation, a wholly owned subsidiary of Lockheed Martin Corporations, for the U.S. Department of Energy's National Nuclear Security Administration under Contract DE-AC04-94AL85000.

models with general forms of linear viscoelastic damping models. The CMS approach is formulated in the physical domain for the solution to transient problems, and each subcomponent is reduced using a Rayleigh-Ritz approach with a set of real, admissible trial vectors obtained from the eigensolution of the undamped equations. A frequency response function (FRF) based substructuring approach was developed by de Lima et al. in [4] where the frequency domain finite element model uses the complex modulus approach and frequency-temperature superposition to capture the frequency and temperature dependent linear viscoelastic behavior. They are concerned with modeling strategies to passively control mechanical vibrations of a main, linear elastic structure connected to linear viscoelastic mounts. The FRF representation allows either of the components to be represented either numerically or experimentally, however no reduction was performed at the subcomponent level. An improvement to the classical Craig-Bampton (CB) substructuring was adapted to viscoelastic finite element models in [5] by computing the fixed-interface and static constraint modes from the frequency independent stiffness and mass matrix, and enriching the basis with static residues associated with the viscoelastic damping forces and external forces. The method was developed for frequency domain responses, and uses a constant modal basis. Tran et al. [6] used a similar method for CMS of vibroacoustic problems, and a free-interface CMS scheme for viscoelastic subcomponents was proposed in [7].

The research presented in this paper develops a fixed-interface CMS approach using primal assembly in the physical domain for linear viscoelastic subcomponent models. Many existing approaches deal solely with frequency based substructuring which can only be solved for steady-state problems. A time domain approach allows the reduced model to be excited via transient inputs or steady state inputs if needed, allowing more flexibility in the types of solutions obtained from the model. Each subcomponent is reduced using a set of linearized complex fixed-interface modes, and a set of pseudo-static constraint modes; this is conceptually similar to the traditional Craig-Bampton approach in [8]. Since the number of interface degrees-of-freedom (DOF) can be prohibitively large, the assembled viscoelastic substructures are further reduced by performing a secondary modal analysis on the assembled boundary. The eigenvectors obtained from this analysis are referred to as linearized complex characteristic constraint modes, and were originally developed for undamped or proportionally damped systems [9, 10].

In Section 2, the fixed-interface CMS theory is developed for linear viscoelastic subcomponents along with the system-level interface reduction. Section 3 presents the results from a numerical example of two sandwich plates assembled at a shared interface. The results for the viscoelastic CMS models with and without interface reduction are presented and show how the results evolve with various bases. The final section draws conclusions from the theory and results.

2. Theoretical Development

A substructuring approach for large scale finite element analysis (FEA) begins by separating the semi-discretized model into smaller subcomponent models. The spatially discretized, N DOF equations of motion for a single subcomponent have the form,

$$\mathbf{M}\ddot{\mathbf{x}} + \mathbf{K}_K \int_0^t \zeta_K(t-\tau)\ddot{\mathbf{x}}(\tau)d\tau + \mathbf{K}_G \int_0^t \zeta_G(t-\tau)\ddot{\mathbf{x}}(\tau)d\tau + \mathbf{K}_e\mathbf{x} = \mathbf{f}_{ext}(t) \tag{1}$$

The coupled integro-differential equations have real, symmetric $N \times N$ matrices $\mathbf{M}$, $\mathbf{K}_K$, $\mathbf{K}_G$, $\mathbf{K}_e$, which correspond to the respective mass, viscoelastic bulk stiffness, viscoelastic shear stiffness, and elastic stiffness. The $N \times 1$ vectors $\mathbf{x}$ and $\mathbf{f}_{ext}(t)$ represent the physical displacements and externally applied forces, respectively, while the overdot is the time derivative. The integrals in Eq. (1) are separated into contributions from the shear and bulk relaxation functions whose constitutive law is represented by an exponential Prony series. The kernel function for the bulk relaxation modulus is written as

$$\zeta_K(t) = \sum_{i=1}^{N_K} K_{coeff,i} e^{-t/\tau_{K,i}} \tag{2}$$

where the leading coefficients must sum to unity

$$\sum_{i=1}^{N_K} K_{coeff,i} = 1 \tag{3}$$

The time-dependent function $\zeta_K(t)$ is a summation of N_K exponential functions that contain an amplitude coefficient $K_{coeff,i}$ corresponding to a particular time constant $\tau_{K,i}$. The shear relaxation kernel function, $\zeta_G(t)$, has the same form as Eqns. (2) and (3), with the exception that the coefficients ($G_{coeff,i}$, $\tau_{G,i}$) will be different and the Prony series may contain a different number of terms (N_G). In general, $\zeta_K(t)$ and $\zeta_G(t)$ are restricted to be continuous and monotonically decreasing, thus requiring that the coefficients and relaxation times be positive (e.g. $K_{coeff,i}$ and $\tau_{K,i}$). The integral terms have a simple functional form, such that the kernel functions are simply a constant matrix multiplied by a series of exponential functions.

Following the classical CB approach, the viscoelastic model in Eq. (1) is partitioned into interior and boundary DOF, respectively corresponding to x_i and x_b.

$$\begin{bmatrix} \mathbf{M}_{ii} & \mathbf{M}_{ib} \\ \mathbf{M}_{bi} & \mathbf{M}_{bb} \end{bmatrix} \begin{Bmatrix} \ddot{\mathbf{x}}_i \\ \ddot{\mathbf{x}}_b \end{Bmatrix} + \begin{bmatrix} \mathbf{K}_{K,ii} & \mathbf{K}_{K,ib} \\ \mathbf{K}_{K,bi} & \mathbf{K}_{K,bb} \end{bmatrix} \int_0^t \zeta_K(t-\tau) \begin{Bmatrix} \dot{\mathbf{x}}_i \\ \dot{\mathbf{x}}_b \end{Bmatrix} d\tau + \begin{bmatrix} \mathbf{K}_{G,ii} & \mathbf{K}_{G,ib} \\ \mathbf{K}_{G,bi} & \mathbf{K}_{G,bb} \end{bmatrix} \int_0^t \zeta_G(t-\tau) \begin{Bmatrix} \dot{\mathbf{x}}_i \\ \dot{\mathbf{x}}_b \end{Bmatrix} d\tau + \begin{bmatrix} \mathbf{K}_{e,ii} & \mathbf{K}_{e,ib} \\ \mathbf{K}_{e,bi} & \mathbf{K}_{e,bb} \end{bmatrix} \begin{Bmatrix} \mathbf{x}_i \\ \mathbf{x}_b \end{Bmatrix} = \begin{Bmatrix} \mathbf{0} \\ \mathbf{f}_{ext}(t) \end{Bmatrix} \tag{4}$$

These subcomponent equations appear conceptually similar to the undamped CB models with the exception of the two integral terms corresponding to the viscoelastic internal forces. The following subsections develop the reduction bases for each subcomponent, the primal assembly step and the interface reduction applied at the system-level.

2.1 Linearized Complex Fixed-Interface Modes

Due to the additional damping terms from the viscoelastic material, the dynamic, fixed-interface modes are obtained by formulating a linearized quadratic eigenvalue problem (QEVP) from the subcomponent model fixed at the entire set of boundary DOF. This is accomplished by retaining only the interior portion of the equations of motion in Eq. (4) as,

$$\mathbf{M}_{ii}\ddot{\mathbf{x}}_i + \mathbf{K}_{K,ii}\int_0^t \zeta_K(t-\tau)\dot{\mathbf{x}}_i d\tau + \mathbf{K}_{G,ii}\int_0^t \zeta_G(t-\tau)\dot{\mathbf{x}}_i d\tau + \mathbf{K}_{e,ii}\mathbf{x}_i = \mathbf{0} \tag{5}$$

Taking the Laplace transform of this equation produces the QEVP,

$$\left(\lambda_r^2\mathbf{M}_{ii} + \lambda_r\mathbf{K}_{K,ii}\sum_{j=1}^{N_K}\frac{K_{coeff,j}}{\lambda_r + 1/\tau_{K,j}} + \lambda_r\mathbf{K}_{G,ii}\sum_{j=1}^{N_K}\frac{G_{coeff,j}}{\lambda_r + 1/\tau_{G,j}} + \mathbf{K}_{e,ii}\right)\boldsymbol{\varphi}_{i,r} = \mathbf{0} \tag{6}$$

The complex scalar λ_r is the eigenvalue while $\boldsymbol{\varphi}_{i,r}$ is the complex eigenvector. As proposed in [11, 12], an iterative approach is used to solve for each complex eigenvector by linearizing the Prony series in Eq. (6) about a prescribed complex value, λ_0,

$$\left(\lambda_r^2\mathbf{M}_{ii} + \lambda_r\mathbf{K}_{K,ii}\sum_{j=1}^{N_K}\frac{K_{coeff,j}}{\lambda_0 + 1/\tau_{K,j}} + \lambda_r\mathbf{K}_{G,ii}\sum_{j=1}^{N_K}\frac{G_{coeff,j}}{\lambda_0 + 1/\tau_{G,j}} + \mathbf{K}_{e,ii}\right)\boldsymbol{\varphi}_{i,r} = \mathbf{0} \tag{7}$$

By linearizing the Prony series about a fixed frequency, $\lambda_0 = i\omega_0$, Eq. (7) is iteratively solved for the r^{th} linearized complex fixed-interface (LC-FI) mode until the residual between computed frequency and linearized frequency is sufficiently small (e.g. $|\mathrm{Im}(\lambda_r) - \omega_0|/|\omega_0| < 10^{-3}$). Due to the frequency dependence of the viscoelastic forces, this process is repeated for each fixed-interface mode of interest. Although there is additional upfront cost to solve the QEVP, the advantage to this approach is the fact that the imaginary part of the eigenvalues exactly corresponds to the oscillation frequency, so the number of fixed-interface modes can be truncated based on a cut-off frequency.

The typical rule of thumb for substructuring is to include modes up to 1.5 to 2.0 times the frequency range of interest, and that rule is recommended for linear viscoelastic models as well.

The set of LC-FI modes are assembled into a complex matrix, $\boldsymbol{\Phi}_{ii}$. Since the basis for reduction in the physical domain is restricted to real vectors, the fixed-interface basis used to reduce Eq. (4) is defined as,

$$\boldsymbol{\Phi}_i^{\mathrm{LC}} = \begin{bmatrix} \mathrm{Re}(\boldsymbol{\Phi}_{ii}) & \mathrm{Im}(\boldsymbol{\Phi}_{ii}) \\ \mathbf{0} & \mathbf{0} \end{bmatrix} \tag{8}$$

Including both the real and imaginary parts of the LC-FI modes essentially doubles the number of shapes, but results in a very efficient basis due to the fact that these account for the viscoelastic forces.

2.2 Pseudo-Static Constraint Modes

As defined by Craig in [13], a static constraint mode is "the static deformation of a structure when a unit displacement is applied to one coordinate of a specified set of constraint coordinates, while the remaining coordinates of that set are restrained, and the remaining degrees-of-freedom of the structure are force-free." For viscoelastic models with time-dependent material laws, the definition by Craig has been extended to the so-called pseudo-static constraint mode (PS-CM). Ignoring the inertia terms in Eq. (4), the frequency domain equations of motion become

$$\left(i\omega \begin{bmatrix} \mathbf{K}_{K,ii} & \mathbf{K}_{K,ib} \\ \mathbf{K}_{K,bi} & \mathbf{K}_{K,bb} \end{bmatrix} \sum_{j=1}^{N_K} \frac{K_{coeff,j}}{i\omega + 1/\tau_{K,j}} + i\omega \begin{bmatrix} \mathbf{K}_{G,ii} & \mathbf{K}_{G,ib} \\ \mathbf{K}_{G,bi} & \mathbf{K}_{G,bb} \end{bmatrix} \sum_{j=1}^{N_G} \frac{G_{coeff,j}}{i\omega + 1/\tau_{G,j}} + \begin{bmatrix} \mathbf{K}_{e,ii} & \mathbf{K}_{e,ib} \\ \mathbf{K}_{e,bi} & \mathbf{K}_{e,bb} \end{bmatrix} \right) \begin{Bmatrix} \mathbf{X}_i \\ \mathbf{X}_b \end{Bmatrix} = \begin{Bmatrix} \mathbf{0} \\ \mathbf{F}_{ext} \end{Bmatrix} \tag{9}$$

A unit displacement at each boundary DOF while holding the others fixed is imposed by setting $\mathbf{X}_b = \mathbf{I}$, where $\mathbf{I}$ is the identity matrix. The interior DOF response to the unit deflection is computed from the top portion of Eq. (9),

$$\left(i\omega \mathbf{K}_{K,ii} \sum_{j=1}^{N_K} \frac{K_{coeff,j}}{i\omega + 1/\tau_{K,j}} + i\omega \mathbf{K}_{G,ii} \sum_{j=1}^{N_G} \frac{G_{coeff,j}}{i\omega + 1/\tau_{G,j}} + \mathbf{K}_{e,ii} \right) \mathbf{X}_i = - \left(i\omega \mathbf{K}_{K,ib} \sum_{j=1}^{N_K} \frac{K_{coeff,j}}{i\omega + 1/\tau_{K,j}} + i\omega \mathbf{K}_{G,ib} \sum_{j=1}^{N_G} \frac{G_{coeff,j}}{i\omega + 1/\tau_{G,j}} + \mathbf{K}_{e,ib} \right) \tag{10}$$

In order to obtain a solution for the PS-CMs, an appropriate frequency, ω, must be chosen. When setting $\omega = 0$, the solution to $\mathbf{X}_i$ results in the classical static constraint mode ($\mathbf{X}_i = -\mathbf{K}_{e,ii}^{-1}\mathbf{K}_{e,ib}$). It is recommended using frequencies $\omega >> 0$, which produce a complex-valued, pseudo-static shape $\mathbf{X}_i$. The real and imaginary parts of these vectors form the set of pseudo-static constraint modes,

$$\boldsymbol{\Psi}_c = \begin{bmatrix} \mathrm{Re}\begin{Bmatrix} \mathbf{X}_i \\ \mathbf{I}_{bb} \end{Bmatrix} & \mathrm{Im}\begin{Bmatrix} \mathbf{X}_i \\ \mathbf{I}_{bb} \end{Bmatrix} \end{bmatrix} = \begin{bmatrix} \mathrm{Re}(\mathbf{X}_i) & \mathrm{Im}(\mathbf{X}_i) \\ \mathbf{I}_{bb} & \mathbf{0} \end{bmatrix} \tag{11}$$

2.3 Subcomponent Model Reduction

The reduced transformation matrix assembles the LC-FI modes from Eq. (8) and the PS-CM from Eq. (11) as,

$$\begin{Bmatrix} \mathbf{x}_i \\ \mathbf{x}_b \end{Bmatrix} = \begin{bmatrix} \mathrm{Re}(\boldsymbol{\Phi}_{ii}) & \mathrm{Im}(\boldsymbol{\Phi}_{ii}) & \mathrm{Im}(\mathbf{X}_i) & \mathrm{Re}(\mathbf{X}_i) \\ \mathbf{0} & \mathbf{0} & \mathbf{0} & \mathbf{I}_{bb} \end{bmatrix} \begin{Bmatrix} \mathbf{q}_k^r \\ \mathbf{q}_k^i \\ \mathbf{x}_b^i \\ \mathbf{x}_b^r \end{Bmatrix} = \mathbf{T}\mathbf{q} \tag{12}$$

The generalized coordinates $\mathbf{q}_k^r$ and $\mathbf{q}_k^i$ correspond to the amplitudes of the real and imaginary parts of the LC-FI shapes, respectively, while $\mathbf{x}_b^r$ and $\mathbf{x}_b^i$ respectively represent the real and imaginary amplitudes of the PS-CMs. The basis in Eq. (12) is projected onto the subcomponent model in Eq. (4), producing a lower order model,

$$\hat{\mathbf{M}}\ddot{\mathbf{q}} + \hat{\mathbf{K}}_K \int_0^t \zeta_K(t-\tau)\dot{\mathbf{q}}(\tau)d\tau + \hat{\mathbf{K}}_G \int_0^t \zeta_G(t-\tau)\dot{\mathbf{q}}(\tau)d\tau + \hat{\mathbf{K}}_e \mathbf{q} = \mathbf{T}^{\mathrm{T}}\mathbf{f}_{ext}(t) \tag{13}$$

where

$$\hat{\mathbf{M}} = \mathbf{T}^{\mathrm{T}}\mathbf{M}\mathbf{T}$$

$$\hat{\mathbf{K}}_K = \mathbf{T}^{\mathrm{T}}\mathbf{K}_K\mathbf{T}$$

$$\hat{\mathbf{K}}_G = \mathbf{T}^{\mathrm{T}}\mathbf{K}_G\mathbf{T}$$

$$\hat{\mathbf{K}}_e = \mathbf{T}^{\mathrm{T}}\mathbf{K}_e\mathbf{T}$$

The real transformation matrix produces real reduced matrices.

2.4 Assembly

The reduced order viscoelastic models attach to adjacent models with a common interface using the primal formulation [2] to satisfy compatibility and equilibrium conditions at the boundary DOF. Without loss of generality, assume that two subcomponents are being coupled, denoted with superscripts (A) and (B). This is accomplished by satisfying the compatibility condition at the real-valued partition of the PS-CMs, such that $\mathbf{x}_b^{r,(\mathrm{A})} = \mathbf{x}_b^{r,(\mathrm{B})}$. This relationship enforces the two boundaries to have the same motion. Following standard assembly methods from finite element analysis [14], a direct coupling matrix $\mathbf{L}$ is defined as,

$$\begin{Bmatrix} \mathbf{q}^{(\mathrm{A})} \\ \mathbf{q}^{(\mathrm{B})} \end{Bmatrix} = \begin{Bmatrix} \mathbf{q}_i^{(\mathrm{A})} \\ \mathbf{x}_b^{r,(\mathrm{A})} \\ \mathbf{q}_i^{(\mathrm{B})} \\ \mathbf{x}_b^{r,(\mathrm{B})} \end{Bmatrix} = \begin{bmatrix} \mathbf{I} & \mathbf{0} & \mathbf{0} \\ \mathbf{0} & \mathbf{0} & \mathbf{I} \\ \mathbf{0} & \mathbf{I} & \mathbf{0} \\ \mathbf{0} & \mathbf{0} & \mathbf{I} \end{bmatrix} \begin{Bmatrix} \mathbf{q}_i^{(\mathrm{A})} \\ \mathbf{q}_i^{(\mathrm{B})} \\ \mathbf{x}_b^{r} \end{Bmatrix} = \begin{bmatrix} \mathbf{L}^{(\mathrm{A})} \\ \mathbf{L}^{(\mathrm{B})} \end{bmatrix} \mathbf{q}_u = \mathbf{L}\mathbf{q}_u \tag{14}$$

The vector $\mathbf{q}_u$ correspond to the unconstrained coordinates of the assembled system. The vectors $\mathbf{q}_i^{(\mathrm{A})}$ and $\mathbf{q}_i^{(\mathrm{B})}$ respectively represent the "interior" portion of the subcomponents (A) and (B) (i.e. those generalized coordinates not belonging to the real valued partition of the PS-CMs). For example, the interior portion of subcomponent (A) consists of $\mathbf{q}_i^{(\mathrm{A})} = [\mathbf{q}_k^{r,(\mathrm{A})^{\mathrm{T}}} \quad \mathbf{q}_k^{i,(\mathrm{A})^{\mathrm{T}}} \quad \mathbf{x}_b^{i,(\mathrm{A})^{\mathrm{T}}}]^{\mathrm{T}}$. Using the coupling matrix in Eq. (14), the reduced order model of the assembled system becomes,

$$\mathbf{L}^{\mathrm{T}} \begin{bmatrix} \hat{\mathbf{M}}^{(\mathrm{A})} & \mathbf{0} \\ \mathbf{0} & \hat{\mathbf{M}}^{(\mathrm{B})} \end{bmatrix} \mathbf{L}\ddot{\mathbf{q}}_u + \mathbf{L}^{\mathrm{T}} \begin{Bmatrix} \hat{\mathbf{K}}_K^{(A)} \int_0^t \zeta_K^{(A)}(t-\tau)\dot{\mathbf{q}}^{(A)}(\tau)d\tau \\ \hat{\mathbf{K}}_K^{(B)} \int_0^t \zeta_K^{(B)}(t-\tau)\dot{\mathbf{q}}^{(B)}(\tau)d\tau \end{Bmatrix} + \mathbf{L}^{\mathrm{T}} \begin{Bmatrix} \hat{\mathbf{K}}_G^{(A)} \int_0^t \zeta_G^{(A)}(t-\tau)\dot{\mathbf{q}}^{(A)}(\tau)d\tau \\ \hat{\mathbf{K}}_G^{(B)} \int_0^t \zeta_G^{(B)}(t-\tau)\dot{\mathbf{q}}^{(B)}(\tau)d\tau \end{Bmatrix} + \mathbf{L}^{\mathrm{T}} \begin{bmatrix} \hat{\mathbf{K}}_e^{(\mathrm{A})} & \mathbf{0} \\ \mathbf{0} & \hat{\mathbf{K}}_e^{(\mathrm{B})} \end{bmatrix} \mathbf{L}\mathbf{q}_u = \mathbf{L}^{\mathrm{T}} \begin{Bmatrix} \mathbf{T}_{CB}^{(\mathrm{A})^{\mathrm{T}}} \mathbf{f}_{ext}^{(\mathrm{A})}(t) \\ \mathbf{T}_{CB}^{(\mathrm{B})^{\mathrm{T}}} \mathbf{f}_{ext}^{(\mathrm{B})}(t) \end{Bmatrix} \tag{15}$$

The form in Eq. (15) is convenient to solve since the integrals can be evaluated at the subcomponent level rather than at the assembly level.

2.5 System-level Interface Reduction

In order to formulate the derivation for the reduction at the interface, Eq. (15) is rearranged such that the unconstrained coordinates, $\mathbf{q}_u$, enter into the integral functions of the viscoelastic forces,

$$\begin{bmatrix} \hat{\mathbf{M}}_{ii}^{(\mathrm{A})} & \mathbf{0} & \hat{\mathbf{M}}_{ib}^{(\mathrm{A})} \\ \mathbf{0} & \hat{\mathbf{M}}_{ii}^{(\mathrm{B})} & \hat{\mathbf{M}}_{ib}^{(\mathrm{B})} \\ \hat{\mathbf{M}}_{bi}^{(\mathrm{A})} & \hat{\mathbf{M}}_{bi}^{(\mathrm{B})} & \hat{\mathbf{M}}_{bb}^{(\mathrm{A})}+\hat{\mathbf{M}}_{bb}^{(\mathrm{B})} \end{bmatrix} \begin{Bmatrix} \ddot{\mathbf{q}}_i^{(\mathrm{A})} \\ \ddot{\mathbf{q}}_i^{(\mathrm{B})} \\ \ddot{\mathbf{x}}_b^r \end{Bmatrix} + \begin{bmatrix} \hat{\mathbf{K}}_{K,ii}^{(\mathrm{A})} & \mathbf{0} & \hat{\mathbf{K}}_{K,ib}^{(\mathrm{A})} \\ \mathbf{0} & \mathbf{0} & \mathbf{0} \\ \hat{\mathbf{K}}_{K,bi}^{(\mathrm{A})} & \mathbf{0} & \hat{\mathbf{K}}_{K,bb}^{(\mathrm{A})} \end{bmatrix} \int_0^t \zeta_K^{(A)}(t-\tau) \begin{Bmatrix} \dot{\mathbf{q}}_i^{(\mathrm{A})} \\ \dot{\mathbf{q}}_i^{(\mathrm{B})} \\ \dot{\mathbf{x}}_b^r \end{Bmatrix} d\tau + \begin{bmatrix} \mathbf{0} & \mathbf{0} & \mathbf{0} \\ \mathbf{0} & \hat{\mathbf{K}}_{K,ii}^{(\mathrm{B})} & \hat{\mathbf{K}}_{K,ib}^{(\mathrm{B})} \\ \mathbf{0} & \hat{\mathbf{K}}_{K,bi}^{(\mathrm{B})} & \hat{\mathbf{K}}_{K,bb}^{(\mathrm{B})} \end{bmatrix} \int_0^t \zeta_K^{(\mathrm{B})}(t-\tau) \begin{Bmatrix} \mathbf{q}_i^{(\mathrm{A})} \\ \mathbf{q}_i^{(\mathrm{B})} \\ \dot{\mathbf{x}}_b^r \end{Bmatrix} d\tau + \ldots$$
$$\begin{bmatrix} \hat{\mathbf{K}}_{G,ii}^{(\mathrm{A})} & \mathbf{0} & \hat{\mathbf{K}}_{G,ib}^{(\mathrm{A})} \\ \mathbf{0} & \mathbf{0} & \mathbf{0} \\ \hat{\mathbf{K}}_{G,bi}^{(\mathrm{A})} & \mathbf{0} & \hat{\mathbf{K}}_{G,bb}^{(\mathrm{A})} \end{bmatrix} \int_0^t \zeta_G^{(A)}(t-\tau) \begin{Bmatrix} \dot{\mathbf{q}}_i^{(\mathrm{A})} \\ \dot{\mathbf{q}}_i^{(\mathrm{B})} \\ \dot{\mathbf{x}}_b^r \end{Bmatrix} d\tau + \begin{bmatrix} \mathbf{0} & \mathbf{0} & \mathbf{0} \\ \mathbf{0} & \hat{\mathbf{K}}_{G,ii}^{(\mathrm{B})} & \hat{\mathbf{K}}_{G,ib}^{(\mathrm{B})} \\ \mathbf{0} & \hat{\mathbf{K}}_{G,bi}^{(\mathrm{B})} & \hat{\mathbf{K}}_{G,bb}^{(\mathrm{B})} \end{bmatrix} \int_0^t \zeta_G^{(\mathrm{B})}(t-\tau) \begin{Bmatrix} \dot{\mathbf{q}}_i^{(\mathrm{A})} \\ \dot{\mathbf{q}}_i^{(\mathrm{B})} \\ \dot{\mathbf{x}}_b^r \end{Bmatrix} d\tau + \begin{bmatrix} \hat{\mathbf{K}}_{e,ii}^{(\mathrm{A})} & \mathbf{0} & \hat{\mathbf{K}}_{e,ib}^{(\mathrm{A})} \\ \mathbf{0} & \hat{\mathbf{K}}_{e,ii}^{(\mathrm{B})} & \mathbf{K}_{e,ib}^{(\mathrm{B})} \\ \hat{\mathbf{K}}_{e,bi}^{(\mathrm{A})} & \hat{\mathbf{K}}_{e,bi}^{(\mathrm{B})} & \hat{\mathbf{K}}_{e,bb}^{(\mathrm{A})}+\hat{\mathbf{K}}_{e,bb}^{(\mathrm{B})} \end{bmatrix} \begin{Bmatrix} \mathbf{q}_i^{(\mathrm{A})} \\ \mathbf{q}_i^{(\mathrm{B})} \\ \mathbf{x}_b^r \end{Bmatrix} = \mathbf{L}^{\mathrm{T}} \begin{Bmatrix} \mathbf{T}_{CB}^{(\mathrm{A})\mathrm{T}} \mathbf{f}_{ext}^{(\mathrm{A})}(t) \\ \mathbf{T}_{CB}^{(\mathrm{B})\mathrm{T}} \mathbf{f}_{ext}^{(\mathrm{B})}(t) \end{Bmatrix} \quad (16)$$

This equation is exactly the same as Eq. (15). The interface reduction corresponds to a secondary modal analysis applied to the boundary DOF partition of the assembly,

$$\left(\hat{\mathbf{M}}_{bb}^{(\mathrm{A})}+\hat{\mathbf{M}}_{bb}^{(\mathrm{B})}\right)\ddot{\mathbf{x}}_b^r + \hat{\mathbf{K}}_{K,bb}^{(\mathrm{A})}\int_0^t \zeta_K^{(A)}(t-\tau)\dot{\mathbf{x}}_b^r d\tau + \hat{\mathbf{K}}_{K,bb}^{(\mathrm{B})}\int_0^t \zeta_K^{(\mathrm{B})}(t-\tau)\dot{\mathbf{x}}_b^r d\tau + \hat{\mathbf{K}}_{G,bb}^{(\mathrm{A})}\int_0^t \zeta_G^{(A)}(t-\tau)\dot{\mathbf{x}}_b^r d\tau + \hat{\mathbf{K}}_{G,bb}^{(\mathrm{B})}\int_0^t \zeta_G^{(\mathrm{B})}(t-\tau)\dot{\mathbf{x}}_b^r d\tau + \left(\hat{\mathbf{K}}_{e,bb}^{(\mathrm{A})}+\hat{\mathbf{K}}_{e,bb}^{(\mathrm{B})}\right)\mathbf{x}_b^r = \mathbf{0} \quad (17)$$

Using the same iterative procedure to compute the LC-FI modes in Section 2.1, the complex modes computed from Eq. (17) produce a set of linearized complex characteristic constraint (LC-CC) modes, denoted as $\boldsymbol{\Psi}_{cc}$. As with the fixed-interface modes, these are also truncated based on frequency, although there is not a well establish rule for an appropriate cut-off frequency. This will be evaluated later in the results section. The LC-CC modes are used to reduce the number of boundary DOF, $\mathbf{x}_b^r$, in Eq. (16) via the transformation,

$$\begin{Bmatrix} \mathbf{q}_i^{(\mathrm{A})} \\ \mathbf{q}_i^{(\mathrm{B})} \\ \mathbf{x}_b^r \end{Bmatrix} = \begin{bmatrix} \mathbf{I} & \mathbf{0} & \mathbf{0} & \mathbf{0} \\ \mathbf{0} & \mathbf{I} & \mathbf{0} & \mathbf{0} \\ \mathbf{0} & \mathbf{0} & \mathrm{Re}(\boldsymbol{\Psi}_{cc}) & \mathrm{Im}(\boldsymbol{\Psi}_{cc}) \end{bmatrix} \begin{Bmatrix} \mathbf{q}_i^{(\mathrm{A})} \\ \mathbf{q}_i^{(\mathrm{B})} \\ \mathbf{q}_{cc}^r \\ \mathbf{q}_{cc}^i \end{Bmatrix} = \mathbf{T}_{cc}\hat{\mathbf{q}}_u \quad (18)$$

Projecting the transformation matrix, $\mathbf{T}_{cc}$, onto Eq. (16) results in the reduced order model of the assembly with interface reduction,

$$\mathbf{T}_{cc}^{\mathrm{T}}\begin{bmatrix} \hat{\mathbf{M}}_{ii}^{(\mathrm{A})} & \mathbf{0} & \hat{\mathbf{M}}_{ib}^{(\mathrm{A})} \\ \mathbf{0} & \hat{\mathbf{M}}_{ii}^{(\mathrm{B})} & \hat{\mathbf{M}}_{ib}^{(\mathrm{B})} \\ \hat{\mathbf{M}}_{bi}^{(\mathrm{A})} & \hat{\mathbf{M}}_{bi}^{(\mathrm{B})} & \hat{\mathbf{M}}_{bb}^{(\mathrm{A})}+\hat{\mathbf{M}}_{bb}^{(\mathrm{B})} \end{bmatrix}\mathbf{T}_{cc}\ddot{\hat{\mathbf{q}}}_u + \mathbf{T}_{cc}^{\mathrm{T}}\begin{bmatrix} \hat{\mathbf{K}}_{K,ii}^{(\mathrm{A})} & \mathbf{0} & \hat{\mathbf{K}}_{K,ib}^{(\mathrm{A})} \\ \mathbf{0} & \mathbf{0} & \mathbf{0} \\ \hat{\mathbf{K}}_{K,bi}^{(\mathrm{A})} & \mathbf{0} & \hat{\mathbf{K}}_{K,bb}^{(\mathrm{A})} \end{bmatrix}\mathbf{T}_{cc}\int_0^t \zeta_K^{(A)}(t-\tau)\dot{\hat{\mathbf{q}}}_u d\tau + \mathbf{T}_{cc}^{\mathrm{T}}\begin{bmatrix} \mathbf{0} & \mathbf{0} & \mathbf{0} \\ \mathbf{0} & \hat{\mathbf{K}}_{K,ii}^{(\mathrm{B})} & \hat{\mathbf{K}}_{K,ib}^{(\mathrm{B})} \\ \mathbf{0} & \hat{\mathbf{K}}_{K,bi}^{(\mathrm{B})} & \hat{\mathbf{K}}_{K,bb}^{(\mathrm{B})} \end{bmatrix}\mathbf{T}_{cc}\int_0^t \zeta_K^{(\mathrm{B})}(t-\tau)\dot{\hat{\mathbf{q}}}_u d\tau + \ldots$$
$$\mathbf{T}_{cc}^{\mathrm{T}}\begin{bmatrix} \hat{\mathbf{K}}_{G,ii}^{(\mathrm{A})} & \mathbf{0} & \hat{\mathbf{K}}_{G,ib}^{(\mathrm{A})} \\ \mathbf{0} & \mathbf{0} & \mathbf{0} \\ \hat{\mathbf{K}}_{G,bi}^{(\mathrm{A})} & \mathbf{0} & \hat{\mathbf{K}}_{G,bb}^{(\mathrm{A})} \end{bmatrix}\mathbf{T}_{cc}\int_0^t \zeta_G^{(A)}(t-\tau)\dot{\hat{\mathbf{q}}}_u d\tau + \mathbf{T}_{cc}^{\mathrm{T}}\begin{bmatrix} \mathbf{0} & \mathbf{0} & \mathbf{0} \\ \mathbf{0} & \hat{\mathbf{K}}_{G,ii}^{(\mathrm{B})} & \hat{\mathbf{K}}_{G,ib}^{(\mathrm{B})} \\ \mathbf{0} & \hat{\mathbf{K}}_{G,bi}^{(\mathrm{B})} & \hat{\mathbf{K}}_{G,bb}^{(\mathrm{B})} \end{bmatrix}\mathbf{T}_{cc}\int_0^t \zeta_G^{(\mathrm{B})}(t-\tau)\dot{\hat{\mathbf{q}}}_u d\tau + \mathbf{T}_{cc}^{\mathrm{T}}\begin{bmatrix} \hat{\mathbf{K}}_{e,ii}^{(\mathrm{A})} & \mathbf{0} & \hat{\mathbf{K}}_{e,ib}^{(\mathrm{A})} \\ \mathbf{0} & \hat{\mathbf{K}}_{e,ii}^{(\mathrm{B})} & K_{e,ib}^{(\mathrm{B})} \\ \hat{\mathbf{K}}_{e,bi}^{(\mathrm{A})} & \hat{\mathbf{K}}_{e,bi}^{(\mathrm{B})} & \hat{\mathbf{K}}_{e,bb}^{(\mathrm{A})}+\hat{\mathbf{K}}_{e,bb}^{(\mathrm{B})} \end{bmatrix}\mathbf{T}_{cc}\hat{\mathbf{q}}_u = \mathbf{T}_{cc}^{\mathrm{T}}\mathbf{L}^{\mathrm{T}}\begin{Bmatrix} \mathbf{T}_{CB}^{(\mathrm{A})\mathrm{T}}\mathbf{f}_{ext}^{(\mathrm{A})}(t) \\ \mathbf{T}_{CB}^{(\mathrm{B})\mathrm{T}}\mathbf{f}_{ext}^{(\mathrm{B})}(t) \end{Bmatrix} \quad (19)$$

3. Numerical Results: Composite Plate Assembly

The substructuring approach is now applied to a numerical example of the assembly of two sandwich plates with viscoelastic foam at the core. Figure 1 shows a schematic of the mesh along with the boundary conditions and interface location. Each plate is modeled with three layers of 20-noded hexahedral elements: the two outer layers correspond to elastic Aluminum 6061-T6 while the interior layer is a viscoelastic PMDI 20 foam. Subcomponent (A) has dimensions of 16 inches by 12 inches by 0.19 inches and a total of 4830 elements (73,605 DOF); subcomponent (B) has dimensions 8 inches by 12 inches by 0.19 inches and a total of 3780 elements (57,855 DOF). For reference, the assembled plate model has a total of 8610 elements or 130,305 DOF. Along the shared interface between the two sandwich plates, there are a total of 1155 DOF. As indicated in Fig. 1, the plates have fixed boundary conditions along the bottom edge and a point load is applied at the free end of the collinear interface.

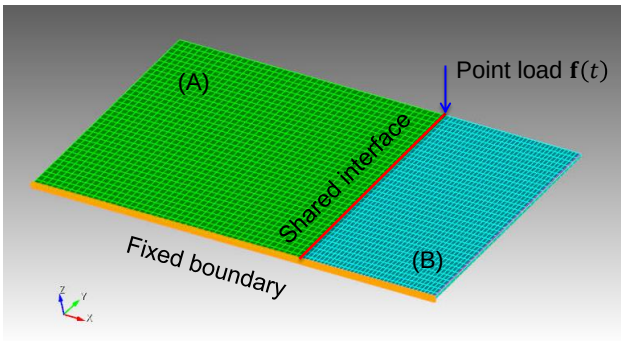

Figure 1. Schematic of finite element mesh for composite sandwich plate with fixed boundary conditions.

3.1 Substructuring with Pseudo-Static Constraint Modes

This first subsection explores the substructuring approach without any reduction at the interface in order to demonstrate the method with the entire physical interface DOF included in the model (i.e. no interface reduction). The driving point FRF is computed for the point load shown in Fig. 1 over the range of 10 to 500 Hz with a frequency step of 1 Hz. These results are shown in Fig. 2. Each subcomponent was reduced with LC-FI modes up to 1000 Hz, two times the frequency bandwidth of interest. The three cases explored are as follows:

1.) Each subcomponent preserves all real and imaginary parts in the reduction basis such that the transformation matrix in Eq. (12) remains as $\mathbf{T} = \begin{bmatrix} \mathrm{Re}(\boldsymbol{\Phi}_{ii}) & \mathrm{Im}(\boldsymbol{\Phi}_{ii}) & \mathrm{Im}(\mathbf{X}_i) & \mathrm{Re}(\mathbf{X}_i) \\ \mathbf{0} & \mathbf{0} & \mathbf{0} & \mathbf{I}_{bb} \end{bmatrix}$.

2.) The imaginary portion of the PS-CMs are removed from the transformation in Eq. (12) such that $\mathbf{T} = \begin{bmatrix} \mathrm{Re}(\boldsymbol{\Phi}_{ii}) & \mathrm{Im}(\boldsymbol{\Phi}_{ii}) & \mathrm{Re}(\mathbf{X}_i) \\ \mathbf{0} & \mathbf{0} & \mathbf{I}_{bb} \end{bmatrix}$.

3.) The imaginary portion of the PS-CMs and LC-FI modes are removed from the transformation in Eq. (12) such that $\mathbf{T} = \begin{bmatrix} \mathrm{Re}(\boldsymbol{\Phi}_{ii}) & \mathrm{Re}(\mathbf{X}_i) \\ \mathbf{0} & \mathbf{I}_{bb} \end{bmatrix}$.

The legend in Fig. 2 labels these three cases respectively as "Full ROM", "No $\mathrm{Im}(\Psi)$", and "No $\mathrm{Im}(\Psi)$ $\mathrm{Im}(\Phi)$".

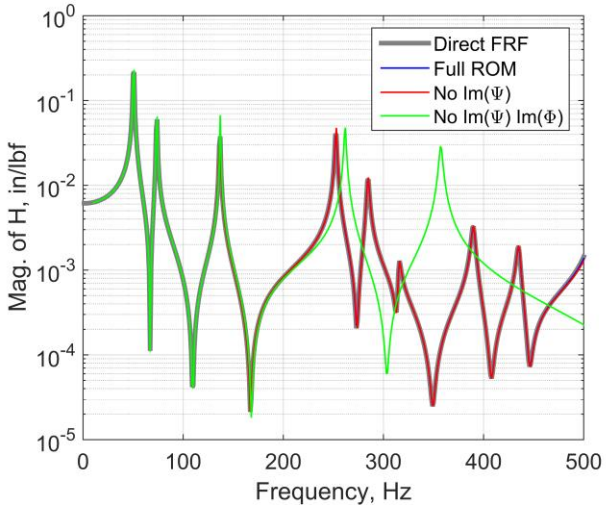

Figure 2. Comparison of driving point FRFs for sandwich plate assembly.

In comparison to the direct FRF computed from the full order model, the "Full ROM" and "No $\mathrm{Im}(\Psi)$" ROM agree very well at the resonances and anti-resonances. It is interesting to note that the imaginary part of the PS-CMs do not significantly improve the results and can be removed from the subcomponent's bases. On the other hand, further removing the imaginary part of the LC-FI modes ("No $\mathrm{Im}(\Psi)$ $\mathrm{Im}(\Phi)$") drastically worsened the accuracy of the ROM. Table 1 shows the order of the models used to compute the FRFs in Fig. 2, along with the required computational time in Matlab to obtain the results. The "No $\mathrm{Im}(\Psi)$" ROM had 1155 fewer DOF than the "Full ROM" and cut the computational time down from 1,070 sec down to 70.4 sec, which was one and three orders of magnitude less than the full model, respectively. As evidenced by the results in Table 1, the solution time does not scale linearly with model size due to the computational effort required to invert larger, dense matrices.

Table 1. Model order and solution time for FRFs in Fig. 2.

Model	Number of DOF	Solution Time
Full FEA Model	130,305	24,050 s
Full ROM	3,495	1,070 s
No $\mathrm{Im}(\Psi)$	1,185	70.4 s
No $\mathrm{Im}(\Psi)$ or $\mathrm{Im}(\Phi)$	1,170	67.8 s

3.2 Substructuring with Interface Reduction

This subsection investigates the interface reduction technique applied to the "No $\mathrm{Im}(\Psi)$" ROM from the previous subsection since this model accurately predicted the driving point FRF with the fewest number of DOF. A total of 13 LC-CC modes were computed from the boundary partition of the assembly in Eq. (17), with the largest natural frequency being 3,993 Hz. This was eight times the frequency band of interest, and was significantly higher compared to the two times frequency rule for the LC-FI modes. Several ROMs with an increasing number of LC-CC modes (keeping both the real and imaginary parts) were created and used to compute the driving point FRFs.

The left plot in Fig. 3 shows the convergence of the FRFs when reducing the interface with the following: 3 LC-CC modes up to 500 Hz, 5 LC-CC modes up to 1000 Hz, 6 LC-CC modes up to 2000 Hz and 13 LC-CC modes up to 4000 Hz. The results from the ROM with 3 LC-CC modes predicted the response well below 300 Hz, but the resonances and anti-resonances were not captured above this frequency. The rest of the ROMs agree quite well with the full order model ("Direct FRF") within 500 Hz, except at some of the anti-resonances. In fact, adding LC-CC modes to the subcomponent bases produced results that converged slowly at these frequencies. At least 13 LC-CC modes up to 4000 Hz were needed to obtain very good agreement between the ROM and the full order model.

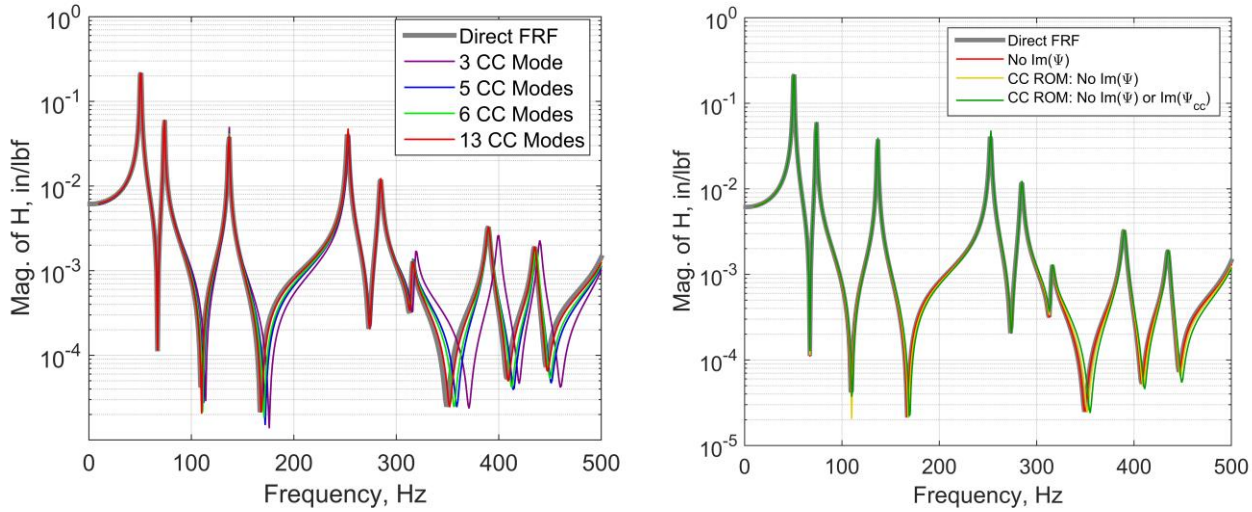

Figure 3. Comparison of driving point FRFs for sandwich plate assembly with interface reduction for (left) varying number of LC-CC modes and (right) 13 LC-CC mode ROMs with and without the imaginary part.

The right plot in Fig. 3 shows a comparison of the driving point FRF for the "No $\mathrm{Im}(\Psi)$" ROM from the previous subsection, along with two ROMs where the interface was reduced with all 13 LC-CC modes. Two cases of these latter models are as follows:

1.) The "CC ROM: No $\mathrm{Im}(\Psi)$" case includes both the real and imaginary parts of all 13 LC-CC modes.

2.) The "CC ROM: No $\mathrm{Im}(\Psi)$ or $\mathrm{Im}(\Psi_{cc})$" case is the same as (1) but removes the imaginary part of the LC-CC modes.

The results from the previous subsection showed that removing the imaginary part of the basis pertaining to the boundary DOF performed very well. This same observation holds true for the LC-CC modes as evidenced by the fact that the "CC ROM: No $\mathrm{Im}(\Psi)$" and "CC ROM: No $\mathrm{Im}(\Psi)$ or $\mathrm{Im}(\Psi_{cc})$" are practically indistinguishable. No difference between the models was observed at the resonant frequencies; however the FRF shifted slightly at the anti-resonances. The results in Table 2 show the size of the models used in Fig. 3b along with the solution time for each. Reducing the interface DOF gained two orders of magnitude in computational savings from the "No $\mathrm{Im}(\Psi)$" ROM, resulting in a total of five orders of magnitude reduction compared to the full order FEA model.

Table 2. Model order and solution time for FRFs in Fig. 3b.

Model	Number of DOF	Solution Time
Full FEA Model	130,305	24,050 s
No $\mathrm{Im}(\Psi)$	1,185	70.4 s
CC ROM: No $\mathrm{Im}(\Psi)$	56	0.4 s
CC ROM: No $\mathrm{Im}(\Psi)$ or $\mathrm{Im}(\Psi_{cc})$	43	0.3 s

3.3 Upfront Computational Cost

All model reduction techniques deserve a discussion of the upfront computational cost required to build the subcomponent models. The Sierra/SD finite element code was only used to compute the LC-FI modes, while a Matlab script was written to compute the PS-CMs and LC-CC modes. When computing complex modes and inverting relatively large matrices, Sierra/SD certainly outperforms Matlab in efficiency, so it makes it difficult to fairly compare the upfront cost. With that comment in mind, the computational effort of each basis is presented in Table 3. The reported values correspond to each code/solver running in serial. Sierra/SD is a massively parallel

structural dynamics FEA code, so using this capability would reduce the computational burden. The upfront costs of these models represent the most upper bound and future work will explore ways to directly compute the PS-CMs and LC-CC modes within Sierra/SD on multiple processors.

Table 3. Upfront cost to compute reduction bases.

Level	**LC-FI Modes**	**PS-CMs**	**LC-CC Modes**
16” x 12” plate	621 s per iteration, per mode (22x621 s = ~4 hours)	37 minutes	N/A
8” x 12” plate	542 s per iteration, per mode (9 x 542 s = ~1.5 hours)	29 minutes	N/A
Assembled Boundary	N/A	N/A	562 s per iteration, per mode (44 x 562 s = ~7 hours)
Code	Sierra/SD	Matlab	Matlab

4. Conclusion

This research developed a fixed-interface component mode synthesis strategy using primal assembly in the physical domain to reduce large-scale finite element models with linear viscoelastic materials. The subcomponent models are reduced using a set of linearized complex fixed-interface modes and pseudo-static constraint modes, each of which account for the internal viscoelastic forces in the equations of motion. Once the models are assembled, the boundary partition, which can be quite large for models with detailed meshes, a secondary complex modal analysis is performed to reduce the number of physical DOF at the interface. The viscoelastic CMS approach is demonstrated on a numerical example of two sandwich plates joined at a common interface. The results show that the ROMs without interface reduction are able to accurately compute the driving point FRFs when compared to the full order model results, as long as the basis includes the imaginary part of the LC-FI modes. The solution time for these models was reduced by three orders of magnitude. When applying the interface reduction with a sufficient number of linearized complex characteristic constraint modes, the ROM preserves the accuracy and lowers the computational cost by five orders of magnitude. It was observed that the frequency cut-off for the LC-CC modes was about eight times the bandwidth of interest, which is significantly higher in comparison to the two times frequency cut-off for the LC-FI modes.

Acknowledgements

This work was supported by the Laboratory Directed Research and Development program at Sandia National Laboratories, a multi-mission laboratory managed and operated by Sandia Corporation, a wholly owned subsidiary of Lockheed Martin Corporation, for the U.S. Department of Energy's National Nuclear Security Administration under contract DE-AC04-94AL85000.

References

[1] R. R. Craig, "Coupling of substructures for dynamic analyses: an overview," in *Proceedings of AIAA/ASME/ASCE/AHS/ASC structures, structural dynamics, and materials conference and exhibit*, 2000, pp. 1573-1584.

[2] D. de Klerk, D. J. Rixen, and S. N. Voormeeren, "General framework for dynamic substructuring: History, review, and classification of techniques," *AIAA Journal,* vol. 46, pp. 1169-1181, 2008.

[3] D. Qian and J. S. Hansen, "A Time Domain Substructure Synthesis Method for Viscoelastic Structures," *Journal of Applied Mechanics,* vol. 62, pp. 407-413, 1995.

[4] A. De Lima, D. Rade, and F. L. Neto, "An efficient modeling methodology of structural systems containing viscoelastic dampers based on frequency response function substructuring," *Mechanical Systems and Signal Processing,* vol. 23, pp. 1272-1281, 2009.

[5] A. M. G. de Lima, A. R. da Silva, D. A. Rade, and N. Bouhaddi, "Component mode synthesis combining robust enriched Ritz approach for viscoelastically damped structures," *Engineering Structures*, vol. 32, pp. 1479-1488, 5// 2010.
[6] Q. H. Tran, M. Ouisse, and N. Bouhaddi, "A robust component mode synthesis method for stochastic damped vibroacoustics," *Mechanical Systems and Signal Processing*, vol. 24, pp. 164-181, 1// 2010.
[7] Z. Ding, L. Li, and Y. Hu, "A free interface component mode synthesis method for viscoelastically damped systems," *Journal of Sound and Vibration*, vol. 365, pp. 199-215, 3/17/ 2016.
[8] R. R. J. Craig and M. C. C. Bampton, "Coupling of Substructures for Dynamic Analysis," *AIAA Journal*, vol. 6, pp. 1313-1319, 1968.
[9] M. P. Castanier, Y. Tan, and C. Pierre, "Characteristic Constraint Modes for Component Mode Synthesis," *AIAA Journal*, vol. 39, pp. 1182-1187, 2001.
[10] R. R. Craig and C. J. Chang, "Substructure Coupling for Dynamic Analysis and Testing," NASA CR-2781, 1977.
[11] R. J. Kuether, K. L. Troyer, and M. R. W. Brake, "Time Domain Model Reduction of Linear Viscoelastic Finite Element Models," presented at the ISMA2016 - International Conference on Noise and Vibration Engineering, Leuven, Belgium, 2016.
[12] Sierra Structural Dynamics Development Team, "Sierra Structural Dynamics-User's Notes," Sandia Report SAND2016-3046 O, 2016.
[13] R. R. J. Craig and A. J. Kurdila, *Fundamentals of Structural Dynamics*, 2nd ed., New York, John Wiley and Sons, 2006.
[14] R. D. Cook, D. S. Malkus, M. E. Plesha, and R. J. Witt, *Concepts and Applications of Finite Element Analysis*, Fourth ed., New York, John Wiley and Sons, 2002.